# Atomic pair distribution function method development at the Shanghai Synchrotron Radiation Facility*

Xiao-Juan Zhou(周晓娟)[1,2,3], Ju-Zhou Tao(陶举洲)[1,2], Han Guo(郭瀚)[4], and He Lin(林鹤)[4,†]

[1] *Institute of High Energy Physics, Chinese Academy of Sciences, Beijing* 100049, *China*
[2] *Dongguan Institute of Neutron Science, Dongguan* 523808, *China*
[3] *University of Chinese Academy of Sciences, Beijing* 100049, *China*
[4] *Shanghai Institute of Applied Physics, Chinese Academy of Sciences, Shanghai* 201204, *China*

(Received 16 October 2016; revised manuscript received 30 March 2017; published online 6 June 2017)

The atomic pair distribution function (PDF) reveals the interatomic distance in a material directly in real-space. It is a very powerful method to characterize the local structure of materials. With the help of the third generation synchrotron facility and spallation neutron source worldwide, the PDF method has developed quickly both experimentally and theoretically in recent years. Recently this method was successfully implemented at the Shanghai Synchrotron Radiation Facility (SSRF). The data quality is very high and this ensures the applicability of the method to study the subtle structural changes in complex materials. In this article, we introduce in detail this new method and show some experimental data we collected.

**Keywords:** atomic pair distribution function, x-ray scattering, local structure, high energy x-ray

**PACS:** 61.05.C–, 61.43.Dq, 61.46.–w **DOI:** 10.1088/1674-1056/26/7/076101

## 1. Introduction

Due to the urgent energy and environmental issues the human race faces today, materials science and synthetic chemistry develop very fast. Artificial functional materials, such as high temperature superconducting materials,[1] new thermoelectric materials,[2] ferroelectric materials,[3] and nanomaterials,[4] are becoming more and more structurally complex. The performance of these materials depends much or solely sometimes on their local atomic structure, but it is very difficult to characterize the local structure of these complex materials on nano and atomic length scales using traditional XRD method because of the generally broad diffuse features present in the diffraction pattern of such materials. Additionally, the traditional XRD method, which is based on the assumption of lattice periodicity and takes into account only the Bragg peaks, can only give the materials' average structure. In recent years, the atomic pair distribution function (PDF) method gained much attention. The PDF method is a total scattering method which takes into account both the Bragg peaks (the global or long range average structure) and diffuse scattering (the local structure) signals, without adding the assumption of lattice periodicity.[5] The diffuse scattering part of a diffraction pattern contains important information regarding the local structure of a material which is generally critical to the material performance. PDF reveals both the short and intermediate range structure of a material.[6] The interatomic distance and the coordination number of atoms in a material are revealed directly in real-space.[7] The atomic instantaneous correlation and the time-independent structure of the system can be derived using energy discriminative and energy non-discriminative signals, respectively.[8]

In the old days, the PDF analysis was a method that people turned to when studying the structure of those materials without long range order, such as amorphous materials like glasses[9] and liquids.[10] Today with the advent of the third generation synchrotron x-ray sources, spallation neutron sources, and high-speed computing, the PDF method developed very fast. People have been using this method to study the disordered, nanocrystallinity and crystallographically challenging materials[6] and nanoscale structural ordering.[11] This method is critical for the study of the amorphous state of materials. It is becoming a very popular and powerful method of characterizing the local structure of various materials. These new third generation synchrotrons and neutron spallation sources, like PETRA-III, DIAMOND, NSLS-II, and SNS, all put PDF as a new technology to be developed with high priority in their new beamline designs.

Other local structure probes, such as extended x-ray absorption fine structure (EXAFS)[12,13] and nuclear magnetic resonance (NMR), give very short-range information. Transmission electron microscopy (TEM) and scanning tunneling microscopy (STM) give the two-dimensional real space pictures of thin samples and surfaces respectively, but currently they do not yield atomic positions with very high precision and usually it is not easy for them to get bulk property of the samples.[5] Compared with these methods, PDF can detect the

*Project supported by the National Natural Science Foundation of China (Grant No. U1232112) and the National Key Basic Research Program of China (Grant No. 2012CB825700).

†Corresponding author. E-mail: linhe@sinap.ac.cn

© 2017 Chinese Physical Society and IOP Publishing Ltd 

distance between atoms up to several or even tens of nanometers accurately. Since peaks in the PDF come directly from bond lengths and other local atomic environment, PDF analysis is very useful in structural studies of nanoscale[11] and disordered materials.[14] However, it has not been widely applied and popularized in China until very recently.[15–19] The main reason is that it is important to measure data to a high value of momentum transfer $Q$ for high real-space resolution of PDF data. Roughly speaking, the spatial resolution $\Delta r \approx \pi/Q_{\max}$, where $Q_{\max}$ is the maximum value of $Q$. Since $Q = 4\pi \sin\theta/\lambda$ ($2\theta$ is the scattering angle), to increase $Q_{\max}$ it is essential to decrease $\lambda$. So the experiments are typically carried out at high-energy synchrotron x-ray sources and pulsed spallation neutron sources with epithermal neutrons of sufficiently high energy.[6] The energy of the electrons in the storage ring of Shanghai Synchrotron Radiation Facility (SSRF) is 3.5 GeV. The high magnetic wiggler at x-ray imaging and biomedical applications beamline (13W) can provide high energy (above 50 keV) x-ray with sufficiently high flux. This makes the high resolution pair distribution function (RAPDF) method possible. For example, the spatial resolution $\Delta r \approx 0.105$ Å when $Q_{\max} = 30.0$ Å$^{-1}$.

## 2. Theoretical derivation for the important PDF formulae

Now we will show the derivation of the PDF equations of most relevance to general users. The full details can be found in Farrow *et al.*[20] We adopt the notations used in the Farrow article since the strict math and consistent convention would be used in the article to avoid the confusion that people can have from reading articles from different fields which generally involve approximations and assumptions obscurely indicated.

The scattering amplitude from a set of $m$ atoms at points $\boldsymbol{r}_m$ in space can be given as

$$\psi(\boldsymbol{Q}) = \sum_m f_m(Q) \exp(\mathrm{i}\boldsymbol{Q}\cdot\boldsymbol{r}_m), \tag{1}$$

where $f(Q)$ is the atomic scattering factor. Then the full coherent scattering intensity is

$$\begin{aligned} I_{\mathrm{coh}} &= \sum_m \sum_n f_n^*(Q) f_m(Q) \exp[\mathrm{i}\boldsymbol{Q}\cdot(\boldsymbol{r}_m - \boldsymbol{r}_n)] \\ &= \sum_{m,n} f_n^*(Q) f_m(Q) \exp(\mathrm{i}\boldsymbol{Q}\cdot\boldsymbol{r}_{mn}). \end{aligned} \tag{2}$$

The self-scattering, $m = n$, can be separated out from $I_{\mathrm{coh}}$ and the remainder, $m \neq n$, is discrete scattering

$$\begin{aligned} I_{\mathrm{dis}} &= I_{\mathrm{coh}} - \sum_m f_m^*(Q) f_m(Q) \\ &= I_{\mathrm{coh}} - N\langle f(Q)^2\rangle \\ &= \sum_{m\neq n} f_n^*(Q) f_m(Q) \exp(\mathrm{i}\boldsymbol{Q}\cdot\boldsymbol{r}_{mn}). \end{aligned} \tag{3}$$

The total scattering structure function is defined as

$$\begin{aligned} S(\boldsymbol{Q}) &= \frac{I_{\mathrm{coh}}}{N\langle f(Q)\rangle^2} - \frac{\langle (f(Q) - \langle f(Q)\rangle)^2\rangle}{\langle f(Q)\rangle^2} \\ &= \frac{I_{\mathrm{coh}}}{N\langle f(Q)\rangle^2} - \frac{\langle f(Q)^2\rangle}{\langle f(Q)\rangle^2} + 1, \end{aligned} \tag{4}$$

where $N$ is the total number of atoms and $\langle\ldots\rangle$ represents an average over all atoms in the sample. Thus, from Eq. (3), we can obtain

$$\begin{aligned} S(\boldsymbol{Q}) - 1 &= \frac{I_{\mathrm{coh}}}{N\langle f(Q)\rangle^2} - \frac{\langle f(Q)^2\rangle}{\langle f(Q)\rangle^2} \\ &= \frac{1}{N\langle f(Q)\rangle^2} \sum_{m\neq n} f_n^*(Q) f_m(Q) \exp(\mathrm{i}\boldsymbol{Q}\cdot\boldsymbol{r}_{mn}). \end{aligned} \tag{5}$$

For an isotropic sample, an orientational average can be taken. Place the $\boldsymbol{Q}$ along $z$, then

$$\begin{aligned} \overline{\exp(\mathrm{i}\boldsymbol{Q}\cdot\boldsymbol{r}_{mn})} &= \frac{\int_0^{2\pi} \mathrm{d}\varphi \int_0^{\pi} \mathrm{d}\theta \exp(\mathrm{i}Qr_{mn}\cos\theta) r_{mn}^2 \sin\theta}{\int_0^{2\pi} \mathrm{d}\varphi \int_0^{\pi} \mathrm{d}\theta r_{mn}^2 \sin\theta} \\ &= \frac{\sin(Qr_{mn})}{Qr_{mn}}. \end{aligned} \tag{6}$$

Thus, for an isotropic sample,

$$S(Q) - 1 = \frac{1}{N\langle f(Q)\rangle^2} \sum_{m\neq n} f_n^*(Q) f_m(Q) \frac{\sin(Qr_{mn})}{Qr_{mn}}. \tag{7}$$

The reduced total scattering structure function $F(Q) = Q[S(Q) - 1]$ is

$$F(Q) = \frac{1}{N\langle f(Q)\rangle^2} \sum_{m\neq n} f_n^*(Q) f_m(Q) \frac{\sin(Qr_{mn})}{r_{mn}}. \tag{8}$$

We now consider the inverse Fourier transform of $F(Q)$ and we call it $f(r)$,

$$\begin{aligned} f(r) &= \frac{2}{\pi} \int_0^{\infty} F(Q) \sin(Qr)\, \mathrm{d}Q \\ &= \frac{2}{\pi} \int_0^{\infty} \frac{1}{N\langle f(Q)\rangle^2} \sum_{m\neq n} f_n^*(Q) f_m(Q) \\ &\quad \times \frac{\sin(Qr_{mn})}{r_{mn}} \sin(Qr)\, \mathrm{d}Q. \end{aligned} \tag{9}$$

We use Morningstar–Warren approximation[21] to separate the $Q$-dependence and the $Q$-independence of $f(Q)$, and then we can gain

$$f(r) = \frac{1}{rN\langle f\rangle^2} \sum_{m\neq n} f_n^* f_m [\delta(r - r_{mn}) - \delta(r + r_{mn})]. \tag{10}$$

If we were confined to the positive axis only,

$$f(r) = \frac{1}{rN\langle f\rangle^2} \sum_{m\neq n} f_n^* f_m \delta(r - r_{mn}). \tag{11}$$

Now we introduce another physical quantity, the radial distribution function (RDF), denoted as $R(r)$. From the definition of RDF, if we choose two bounds, $a$ and $b$, the integral of

the RDF between them gives the number of atomic pairs per atom, $N_{ab}$. From Eq. (11), if we multiply $f(r)$ by $r$, we can find

$$\int_a^b rf(r)\,\mathrm{d}r = \int_a^b \frac{1}{N\langle f\rangle^2}\sum_{m\neq n} f_n^* f_m \delta(r-r_{mn})\,\mathrm{d}r = \frac{1}{N\langle f\rangle^2}\sum_m \sum_{n\in S} f_n^* f_m, \tag{12}$$

where $S$ is the set of atoms with distance between $a$ and $b$ from atom $m$. If the sample has just one atomic species, this reduces to

$$\int_a^b rf(r)\,\mathrm{d}r = \frac{f^2}{f^2}\sum_{n\in S} 1 = N_{ab}. \tag{13}$$

Thus

$$R(r) = rf(r) = 4\pi r^2 \rho(r), \tag{14}$$

$$\rho(r) = \frac{1}{4\pi r^2 N\langle f\rangle^2}\sum_{m\neq n} f_n^* f_m \delta(r-r_{mn}). \tag{15}$$

In reality, due to the experimental instrument design, $I_{\mathrm{coh}}(Q)$ is measured down to a minimum $Q_{\min}$ and we also have a finite $Q_{\max}$, so the PDF, $G(r)$, is obtained experimentally in most case. $G(r)$ is related to the measured x-ray or neutron powder diffraction data, that is

$$G(r) = \frac{2}{\pi}\int_{Q_{\min}}^{Q_{\max}} Q[S(Q)-1]\sin(Qr)\,\mathrm{d}Q = \frac{2}{\pi}\int_{Q_{\min}}^{Q_{\max}} F(Q)\sin(Qr)\,\mathrm{d}Q = 4\pi r\rho(r) - \frac{2}{\pi}\int_0^{Q_{\min}} F(Q)\sin(Qr)\,\mathrm{d}Q. \tag{16}$$

The second part of the above equation represents the small angle scattering intensity and we disregarded the part above the $Q_{\max}$ since it results in spurious oscillations. The termination at $Q_{\max}$ broadens the PDF, since zero-point vibration and thermal motion of atoms are physically unavoidable and they always give finite broadening effects on the PDF peaks, a minimum value for $Q_{\max}$ can be chosen so that we can ignore the broadening effect coming from finite $Q_{\max}$ when its effect is small enough compared to the other two.[8] Thus, for bulk crystals in which the region of interest in the PDF is usually much smaller than the smallest dimension of the crystal,

$$G(r) = 4\pi r(\rho(r) - \rho_0), \tag{17}$$

where $\rho(r)$ is the pair density function and $\rho_0$ is the number density of the material.

## 3. Synchrotron x-ray PDF experiments

### 3.1. Experimental setup

In the early days of PDF experiment, a diffractometer was needed since it provides high $2\theta$ needed to get higher $Q$ when the x-ray energy is relatively low. The scan mode limits the data collection speed and the medium or low energy x-ray available in the old days greatly limits the resolution of the method due to the relative low $Q_{\max}$. Today a synchrotron radiation x-ray PDF experiment usually requires a large area detector like an image plate or Perkin Elmer silicon detector and high-energy x-ray ($E$>50 keV) for fast data collection, which is the so-called high-energy PDF or Rapid PDF (RAPDF) experiment.[22] Figure 1 is the simple schematic of the experimental setup. The lead shielding plate with a small hole in the middle was made up of a lead plate of about 1 mm thickness in the middle for shielding and thin aluminum slides on both sides for easy handling. Most large area detectors used in synchrotron radiation facilities have no energy discrimination, so the PDF obtained in this way can be understood as approximate instantaneous atomic correlation function.

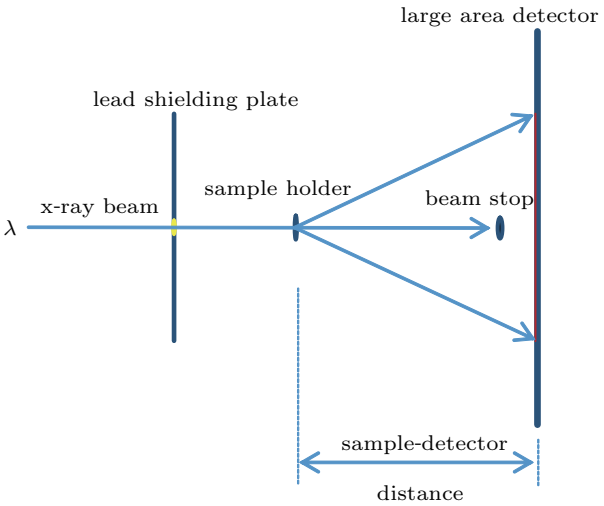



**Fig. 1.** Simple schematic of the PDF experimental setup.

The PDF experiments were done at SSRF 13W beamline (BL). Currently the BL13W is the only beamline that can deliver high energy ($E > 50$ keV) x-ray flux in the SSRF using a 1.9 Tesla wiggler. The source size is 408 μm × 23 μm and the divergence is 5.14 mrad×0.15 mrad. BL13W is an unfocused beamline with simple optics setup. Two flat double crystal monochromators placed at 28 meters away from the source can be switched to select either regular hard x-ray (Si (111)) or high energy x-ray (Si (311)).

Although the Si (111) can give much higher intensity since the reflectivity is higher compared with the Si (311), in the high energy range we use the Si (311) because the beamline is dedicated to the imaging purpose and low incident angle limit is taken to avoid damage of the monochromators.

The total photon energy is in the range of 8–72.5 keV and the energy resolution is better than $5\times10^{-3}$ even in the high energy end. The output flux can reach $2\times10^8$ phs/s/mm$^2$ when the energy is 70 keV. Before doing PDF experiments, the beam size was adjusted to about 1 mm or smaller in most

cases when the window of x-ray incoming is small by using 2 slits: a white beam slit and a monochromator slit located at 20 m and 30 m away from the source, respectively. The distance between the source and sample depends on the specific experiment to be performed. When doing a regular experiment at room temperature, the sample holder is a thin aluminum plate with a diameter 1 cm in the middle, and the bottom is an aluminum cylindrical bearing. The distance between source point and sample is about 34 m. When doing *in situ* experiments or low temperature experiments, the distance between source point and sample is around 36 m. The plate (as shown in Fig. 1), the sample holder, and the detector are free to move utilizing the sliding platform design on the optics table, so the plate and the sample holder can get close to suppress the scattering of stray light, and the sample holder and the detector can get close to increase the scattering angle and reduce the air scattering under the premise of not affecting the experimental data.

In summary, the experimental setup for PDF at SSRF is very simple. It does not have a focusing device and uses a flat crystal monochromator to select high-energy x-ray, which makes it easy to analyze the optical properties (such as divergence) of the x-ray used and also gives a relatively high resolution in $Q$ space.

Below we show several typical experiment examples.

### 3.2. Room temperature PDF experiment on nickel powder

#### 3.2.1. Experimental process

Pure nickel (Ni) is chosen as a standard sample to test the quality of our PDF data because Ni has a simple fcc structure. A lead plate with a small hole in the middle was placed before the sample container during experiments in order to suppress stray light as said before. The energy used was 69.525 keV ($\lambda = 0.17835$ Å) and calibration of energy at 69.525 keV was achieved using the tungsten absorption edge. In order to protect the detector, a beam stop is also used to block the direct beam. Decreasing the distance between sample and detector is an effective way to increase $Q_{\max}$, but short distance requires a small beam stop in order to avoid blocking the inner diffraction rings. On the other hand, too small a beam stop can also increase difficulty in the aligning process. Under the comprehensive consideration, a suitable size of beam stop should be chosen. The size of beam stop we used is about 8 mm and this causes a valid minimum value of $Q$ of about 1.0 Å$^{-1}$ (the sample-to-detector distance is about 110 mm). In the alignment process, a Marcam is a useful tool to observe the size and shape of the x-ray to ensure that the x-ray does not hit the other things of the container. The raw data measured from Ni is shown in Fig. 2. The detection time of Ni was 90 s and it varied with samples. Usually it is necessary to repeat a number of times until the statistical errors/noise are acceptable in the high $Q$ range since the detector can saturate in one simple exposure/scan. We used two layers of kapton tape to paste the sample into the sample holder. The reason why we use kapton tape is that it has a weak background. The intensities from an empty container plus two layers of kapton tape were also measured as the background to be subtracted. A $CeO_2$ standard sample was used to calibrate the sample-to-detector distance.

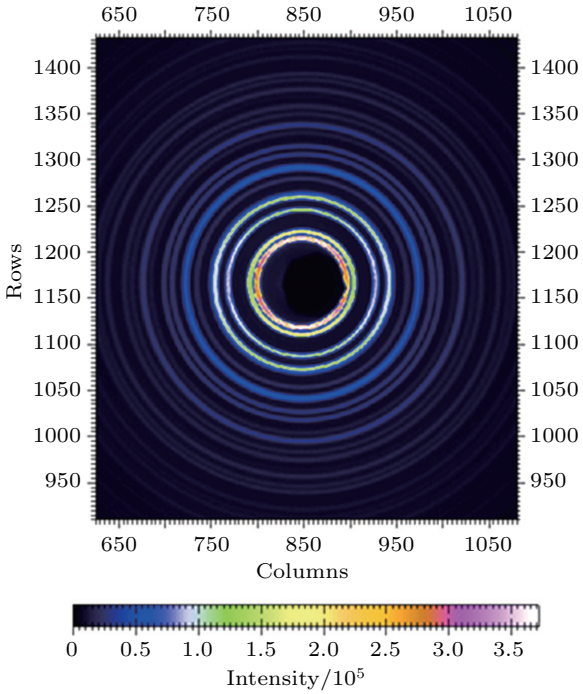



**Fig. 2.** The two-dimensional contour map of Ni powder from large area detector.

#### 3.2.2. Data processing

The software Fit2D[23] was used to integrate all raw data and converted them to intensity versus $2\theta$ (the angle between the incident and scattered x-rays). Then the integrated data were transferred to a program PDFgetX3,[24] through standard corrections and background subtraction to obtain PDF, as displayed in Fig. 3. There are some small ripples in Fig. 3(c) before the first PDF $G(r)$ peak at $r = 2.4$ Å. These ripples come from the imperfect corrections and the ripples' amplitudes are very small which is a good indication that the data is of high quality.[22] There are currently two popular programs available to obtain PDF: PDFgetX2[25] and PDFgetX3. The main difference between them is that PDFgetX2 requires more professional knowledge about x-ray scattering for data process and PDFgetX3 requires little user input and is highly automatable, but the results are the same when processed correctly except for an arbitrary constant coefficient.[24]

There is certainly other software used by different groups before even PDFgetX2 was written. In the authors' opinion, PDFgetX2 and PDFgetX3 gained popularity because of the development of the software science. PDFgetX3 got especially successful large attributes to the open source frame.

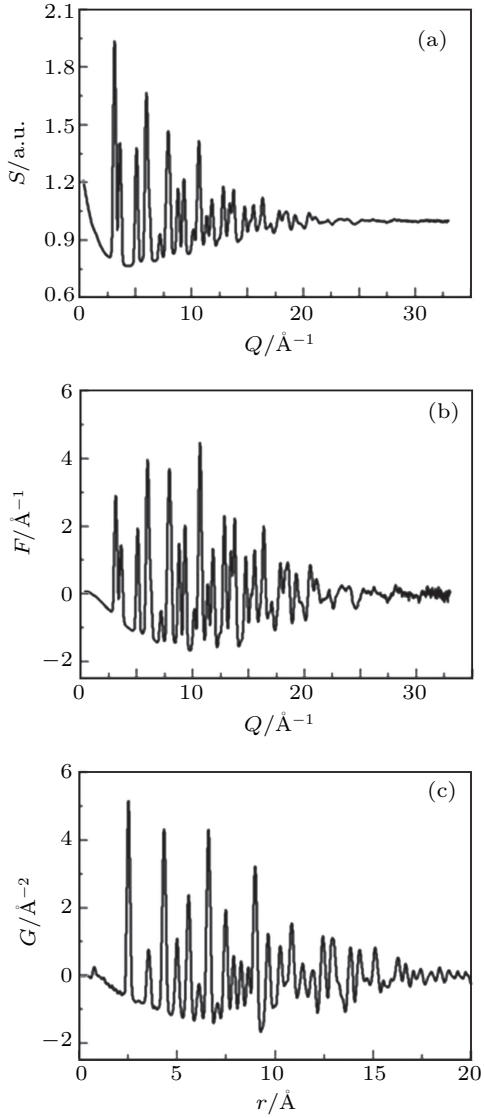



**Fig. 3.** (a) The total scattering structure function $S(Q)$, (b) the reduced total scattering structure function $F(Q)$, and (c) the PDF $G(r)$ of Ni ($Q_{max} = 33.0$ Å$^{-1}$).

### 3.3. In situ PDF experiment on thermoelectric material $Cu_2Se$

We have optimized the experimental setup for the low and high temperature experiments. Since the opening of high and low temperature apparatus for incoming x-rays is usually small, it can be a difficult task to do beam alignment. We used high precision translation stage and lifting platform coupled with a Marcam to regulate and align the x-ray path. In high-temperature experiments, gases such as argon or nitrogen can fill the sample chamber to protect the sample from oxidation. The gas from the gas outlet can be recycled to blow into the surface of the sample chamber to avoid ice freezing in the process of low-temperature experiments. $Cu_2Se$ sample was measured at different temperatures using the linkam heating/cooling stage. Data are shown at three temperature points: low temperature (86 K), room temperature (300 K), and high temperature (420 K) since phase transition occurs at about 400 K. The detection times were 200 s, 240 s, and 250 s, respectively. The changes of PDF are significant in Fig. 4. This set of devices has been used by Lin *et al.* to study the change of local structure of nanocrystalline GaNMn3-BM0 and GaNMn3-BM25 due to ball milling (the BM0 and BM25 mean 0-h and 25-h ball milling, respectively).[16]

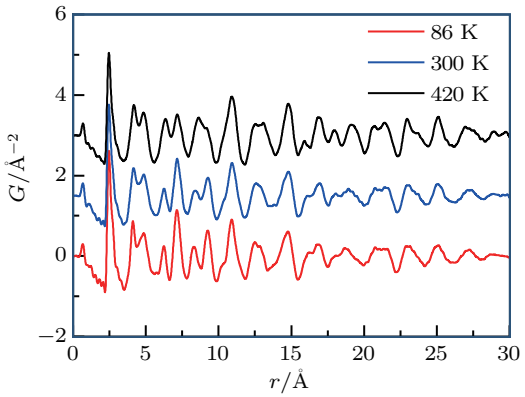



**Fig. 4.** PDFs from $Cu_2Se$ at temperature 86 K (red), 300 K (blue), and 420 K (black). $Q_{max} = 25.0$ Å$^{-1}$.

## 4. Data refinement process

Although we have shown the experimental data of two kinds of materials, we just show the refinement results of Ni. The program PDFgui[26] was used to refine the structure of Ni. PDFgui is a program which can be used to refine crystal structures in real space based on experimental PDF data. It can fit multiple structures if a material has different structure phase. Many variables are included in the structure phase, such as lattice constants, anisotropic atomic displacement parameters (ADPs), atomic site occupation, data and phase scale factors, and a set of parameters which have relation to atomic motion effects or scatter size effects in the PDF. Another advantage is that this program supports space group operations. Once the space group is specified, the program can expand an asymmetric unit to a full cell and can also generate symmetry constraints for atomic ADPs and atomic coordinates according to the symmetry requirements.[27] The simulation results are shown in Fig. 5 and the $Rw$ ($Rw = \sqrt{\{\sum_{m=1}^{N}[G_{exp}(r_m) - G_{theory}(r_m)]^2 / \sum_{m=1}^{N} G_{exp}^2(r_m)\}}$, where $G_{exp}$ and $G_{theory}$ are the experimental PDF and theoretical PDF, respectively) value is 0.082 (when $Q_{max} = 33.0$ Å$^{-1}$).

When compared with the PDF experiments at the MU-CAT 6-ID-D beamline at Advanced Photon Source (APS), Argonne National Laboratory, the main differences are shown in Table 1 (the APS PDF experimental data is derived from PDFgui user guide). Although the energy is relatively low in our experiment, the $Q_{max}$ value of 33 Å$^{-1}$ is sufficient for accurate determination of the PDF, since for most materials the influence of thermal vibration is dominant as mentioned before except at very low temperatures.[8] The $Q_{max}$ value can also be

increased even higher if we decrease the distance between the sample and the detector.

**Table 1.** Comparison of experimental data between APS and SSRF.

| | $E$/keV | $Q_{max}/Å^{-1}$ | Cell parameters/Å | $U_{iso}/Å^2$ | $Rw$ |
|---|---|---|---|---|---|
| APS | 98.001 | 40 | 3.5316 | 0.00545 | 0.075 |
| SSRF | 69.525 | 33 | 3.5119 | 0.00490 | 0.082 |

The crystal structure of nickel from Crystallography Open Database (COD ID: 9013024) gives the cell parameter 3.524 Å ($a = b = c$). Different structure files have different values of the isotropic atomic displacement parameters ($U_{iso}$) and we use 0.0025 Å$^2$ as the initial value in the refinement.

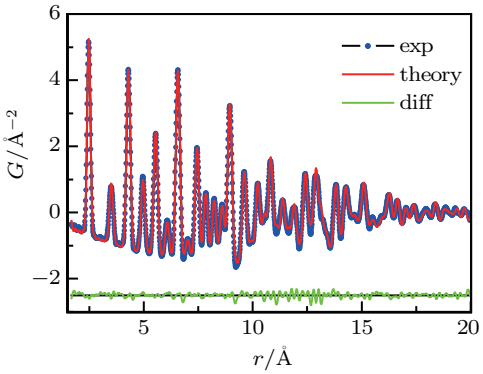



**Fig. 5.** The experimental $G(r)$ (blue) and the theoretical $G(r)$ (red) from the structure model of Ni powder. The difference curve is shown offset below (green).

For disordered materials, reverse Monte Carlo (RMC) method is a useful method to analyze the atomic structure since it considers both the atomic positions and their correlations. A Monte Carlo algorithm is used in the process of constructing the atomic model and configurations will be produced finally, which are in best agreement with experimental data. Moreover, there are no parameterized equations that drive the model because experimental data are used directly in this process at all stages.[28] Now someone has used the method of density function theory coupled with PDF to explore the structure of materials.[29–31]

## 5. Low-temperature PDF

Low-temperature PDF method is very important for condensed matter physics research. Many materials such as superconductors and other strong correlated systems need to be studied at low-temperature (below the nitrogen boiling point) environment. Two solutions satisfy this need. One is to cool the sample as in bio-XRD experiments, i.e., blowing cooling gas (nitrogen or helium) to the sample. An N-HeliX system from Oxford Cryosystems company, which can cool the sample down to 28 K, is equipped at SSRF. This system has the merit of easy sample changing and minimized background. But it cannot reach temperatures below 25 K.

Another way to do a low temperature PDF experiment in which the temperature can reach below 25 K is to use the cryostat system. If the sample is held in the cryostat, a wide scattering angle for the x-ray generally means a big opening for the sample chamber and consequently big heat loads from thermal radiation on the cryogenic system. This puts high requirements for both the cooling power and the thermal shielding design.[32] We designed a dedicated sample chamber for PDF experiment. The cryocooler (DE-202SG) and the compressor provided by the Advanced Research System (ARS) Company can be mounted on the Huber diffractometer, suitable not only for PDF experiment but also for other low-temperature experiments. We should note that helium in both the cryostream and the ARS system is run in a closed cycle. Such systems have the advantage of minimum helium loss (or lossless in helium).

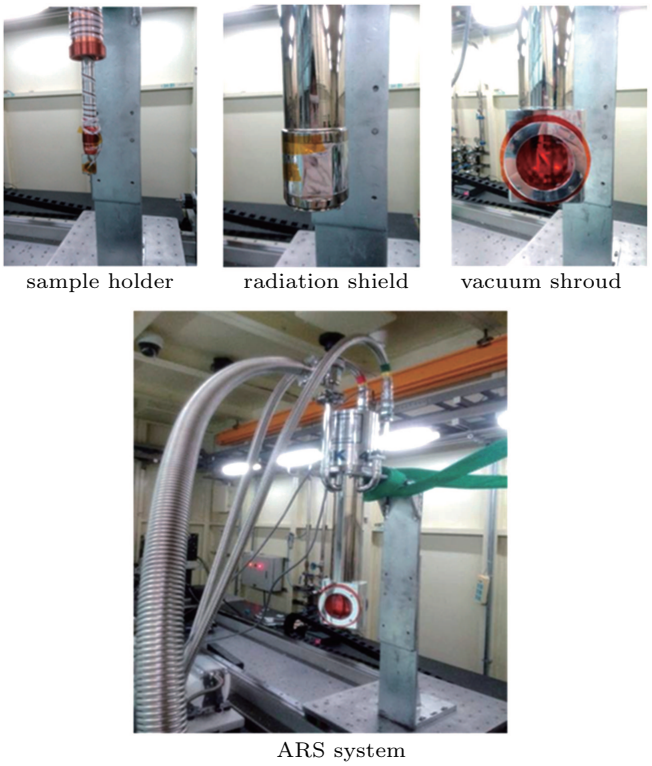



**Fig. 6.** The cryogenic device.

The ARS system has a large exit window that covers 70° of $2\theta$ angle. With this system, the sample can reach as low as 15 K. If the energy of the x-ray is 70 keV, $Q_{max} > 40$ Å, a reliable value to detect materials' low temperature structure accurately. The chamber has a coldhead in contact with the sample holder in the innermost layer, radiation shield in the middle, and vacuum shroud in the outermost layer. The sample holder is a copper plate with a hole in the center and the size of the sample holder window is 0.5 inches in diameter. The radiation shield window was covered by one aluminized mylar layer in order to shield the thermal radiation and minimize the heat load on the sample and coldhead.[32]

The thickness of mylar is 6 μm, with aluminum thickness of roughly 50 nm. The window material of the vacuum shroud was kapton since it contributes a weak background and has good strength to sustain the atmosphere pressure. The distance from sample to vacuum shroud window is 0.51 inches and the diameter for the outgoing window is about 3 inches. The scattering angle for the outgoing x-ray can reach 70 degrees. The size of kapton window in the incoming side of the x-ray is 1.5 inches in diameter with 1.25 inches clear-view. The thickness of the kapton is 0.005 inches. Figure 6 shows the picture of the cryogenic device. The nickel powder was pressed into a slice and we used it to do the low-temperature experiments. The results of 35.3 K were shown in Fig. 7 and Table 2 lists all refinement results. Table 2 depicts that the cell parameters increase with increasing temperature owing to thermal expansion. The isotropic atomic displacement parameters increase with increasing temperature. The values of *Rw* increase a bit while the temperature decreases since the truncation errors become more severe.

**Table 2.** Crystal structure data from PDFgui refinement for Ni at different temperatures ($T$ is the stabilized temperature of the sample rather than the coldhead).

| $T$/K | $a/b/c$/Å | $U_{iso}$/Å$^2$ | *Rw* |
|---|---|---|---|
| 35.3 | 3.5080 | 0.00130 | 0.069 |
| 55.8 | 3.5082 | 0.00137 | 0.071 |
| 100.5 | 3.5091 | 0.00162 | 0.063 |
| 188.9 | 3.5137 | 0.00263 | 0.048 |
| 287.1 | 3.5217 | 0.00433 | 0.046 |

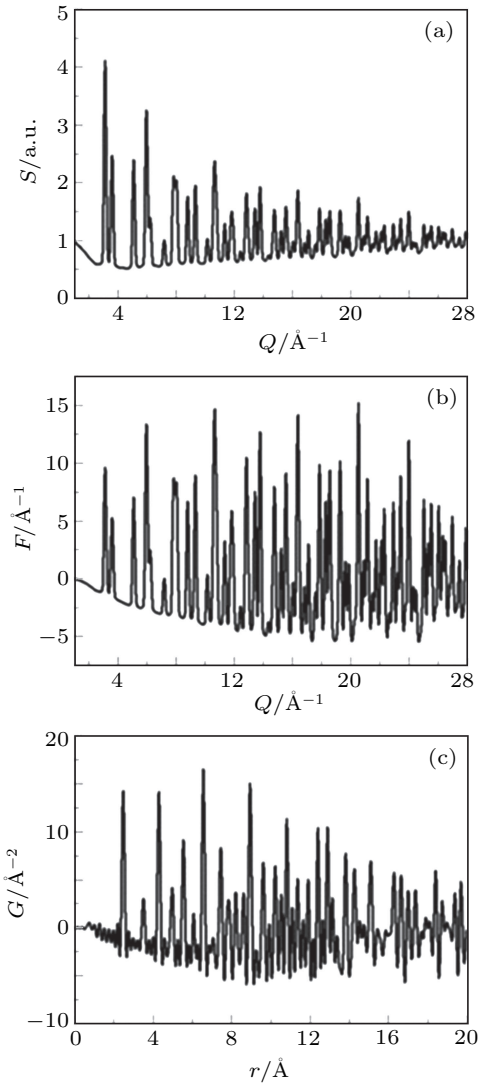



**Fig. 7.** (a) The total scattering structure functions $S(Q)$, (b) the reduced total scattering structure functions $F(Q)$, and (c) the PDF $G(r)$ of Ni at 35.3 K ($Q_{max} = 28.0$ Å$^{-1}$).

## 6. Some key technique developments crucial to PDF method development

One development is to combine PDF with another method. It would be great to collect both the small angle scattering signal and higher $Q$ signal for PDF simultaneously in the experiment.[20] Technically, it is now possible to make a scatterless pinhole for high-energy x-rays. Given proper alignment of the pinholes and the beam stop, it would be possible to measure SAXS and PDF signal in one experiment and this is very important for the nano-sized samples.

In the algorithm part, combining information from XAFS and PDF method in the data analysis process might be quite interesting. XAFS is a natural complementary method to PDF as a local structure analysis method. *Ab initio* reconstruction method generated much interest.[33,34] We should expect better starting structure for the structure searching process, faster converging, and more reasonable final structure after putting the constraint in the reconstruction. Putting a constraint from SAXS signal into the reconstruction algorithm might also be helpful.

Anomalous PDF method using the change of atomic scattering factors near absorption edges is very interesting since it can distinguish directly if an atom/ion species contributes to a given atomic pair distance. Instrument development in a synchrotron station is probably the most important for an anomalous PDF method using high-energy x-ray. High-energy resolution is not easy to implement in the high-energy case. The article by Shastri describes one scheme in which bent Laue crystal (premonochromator), compound refractive lenses (collimator), and double flat Bragg crystal (monochromator) are combined together to give a very high-energy resolution for the high-energy x-rays.[35]

For those PDF experiments when the micro-sized beam is required, like when a diamond anvil cell is needed for high pressure, focusing the high-energy x-ray is usually necessary to guarantee enough photon flux. This is a general topic for high-energy x-ray and would not be discussed here. It is though important to know that different sources (undulator or wiggler) might require a totally different focusing scheme using totally different x-ray optics elements.[36,37]

Very recently, detectors optimized for high energy photon detection using CdTe as a sensor are finally emerging in the market. This would have a huge impact for high-energy x-ray science. For decades, the relatively low efficiency of the high-energy x-ray detector has limited this field to a large degree. With pretty high quantum efficiency and very fast data readout speed, the field of high-energy scattering is to be changed. So far the detector still does not have energy resolution that can eliminate the Compton scattering signal which still has to be theoretically ruled out. The key parameter $Q_{\max}$ that determines the real space resolution in PDF is expected to be extended even larger with improvement in detector and x-ray optics.[8,38] Many science questions that remain ambiguous or controversial due to limitation in the resolution issue of PDF data could be finally solved. A note worth mentioning is that for a total scattering method like PDF it is crucial to pick a large-area detector with uniform response to x-ray, which would require a uniform response of both sensor and follow-up electronics, otherwise the $Q$ range accessible would be largely deduced, since an abrupt signal jump in $Q$ space caused by detector flaw might lead to serious problems in data analysis.

## 7. Outlook of PDF method at SSRF

In this section, we will talk about the current effort and future development of PDF in SSRF.

There are many things that can be done for the future development of the PDF method in SSRF. These will mainly be driven by the users' needs. In ab initio chemical reaction experiment, high-energy x-ray can penetrate the container wall or window more easily and PDF can give useful local structure information during the reaction process. PDF method can be combined with a high-pressure technique to study the behavior of systems under extreme conditions. As mentioned before, this will require focusing of the high-energy x-ray to micro size. This is one major work we are putting much effort into now. Different focusing elements, like CRL, Sawtooth, and kinoform lens, will be either purchased or made. Different levitation techniques suitable for varied systems can also be combined with the high-energy PDF method to study those processes that require containerless conditions.[39,40] This is very important for such studies on high-temperature liquid, supercooled (metastable) liquid, and even pharmaceutical drug studies.

## Acknowledgment

We thank Dr. Doug Robingson (APS) for his valuable advice in the cryostat design. Help from Dr. S. D. Shastri (APS) is also appreciated in the discussion of high-energy x-ray focusing. We also thank other members at SSRF BL13W for help in the high-energy x-ray experiment.

## References

[1] Billinge S J L, Kwei G H and Takagi H 1994 *Phys. Rev. Lett.* **72** 2282
[2] Lin H, Bozin E S, Billinge S J L, Androulakis J, Malliakas C D, Lin C H and Kanatzidis M G 2009 *Phys. Rev. B* **80** 045204
[3] Petkov V, Buscaglia V, Buscaglia M T, Zhao Z and Ren Y 2008 *Phys. Rev. B* **78** 054107
[4] Masadeh A S, Bozin E S, Farrow C L, Paglia G, Juhas P, Billinge S J L, Karkamkar A and Kanatzidis M G 2007 *Phys. Rev. B* **76** 115413
[5] Egami T and Billinge S J L 2003 *Underneath the Bragg Peaks: Structural Analysis of Complex Materials* (Oxford: Elsevier) pp. 25–49
[6] Billinge S J L and Kanatzidis M G 2004 *Chem. Commun.* **2004** 749
[7] Warren B E 1969 *X-ray Diffraction* (New York: Dover) pp. 116–123
[8] Toby B H and Egami T 1992 *Acta Cryst. A* **48** 336
[9] Cargill G S III 1975 *Solid State Phys.* **30** 227
[10] Narten A H, Thiessen W E and Blum L 1982 *Science* **217** 1033
[11] Billinge S J L 2008 *J. Solid State Chem.* **181** 1695
[12] Lu K Q 1985 *Prog. Phys.* **1** 125
[13] Sayers D E, Stern E A and Lytle F W 1971 *Phys. Rev. Lett.* **27** 1204
[14] Jeong I K, Graf M J and Heffner R H 2005 *J. Appl. Cryst.* **38** 55
[15] Yu Q, Wang X D, Lou H B, Cao Q P and Jiang J Z 2016 *Acta Mater.* **102** 116
[16] Lin J C, Tong P, Zhou X J, Lin H, Ding Y W, Bai Y X, Chen L, Guo X G, Yang C, Song B, Wu Y, Lin S, Song W H and Sun Y P 2015 *Appl. Phys. Lett.* **107** 131902
[17] Li F, Yuan J S, Li D C, Li S Y and Han Z 2015 *J Mol Struct* **1081** 38
[18] Ahmad A S, Zhao X N, Xu M X, Zhang D X, Hu J W, Fecht H J, Wang X D, Cao Q P and Jiang J Z 2017 *J Low Temp Phys* **186** 172
[19] Guo X G, Lin J C, Tong P, Wang M, Wu Y, Yang C, Song B, Lin S, Song W H and Sun Y P 2015 *Appl. Phys. Lett.* **107** 202406
[20] Farrow C L and Billinge S J L 2009 *Acta Cryst. A* **65** 232
[21] Warren B E, Krutter H and Morningstar O 1936 *J. Am. Ceram. Soc.* **19** 202
[22] Chupas P J, Qiu X Y, Hanson J C, Lee P L, Grey C P and Billinge S J L 2003 *J. Appl. Cryst.* **36** 1342
[23] Hammersley A P, Svenson S O, Hanfland M and Hauserman D 1996 *High Pressure Res.* **14** 235
[24] Juhas P, Davis T, Farrow C L and Billinge S J L 2013 *J. Appl. Cryst.* **46** 560
[25] Qiu X Y, Thompson J W and Billinge S J L 2004 *J. Appl. Cryst.* **37** 678
[26] Farrow C L, Juhás P, Liu J W, Bryndin D, Bozin E S, Bloch J, Proffen T and Billinge S J L 2007 *J. Phys. -Condens. Matter* **19** 335219
[27] Farrow C L, Juhás P, Liu J W, Bryndin D, Bozin E S, Bloch J, Proffen T and Billinge S J L 2009 *PDFgui User Guide* pp. 9–13
[28] Tucker M, Dove M, Goodwin A and Keen D 2012 *RMCProfile User Manual* pp. 4–7
[29] Shi C Y, Beidaghi M, Naguib M, Mashtalir O, Gogotsi Y and Billinge S J L 2014 *Phys. Rev. Lett.* **112** 125501
[30] Rademacher N, Bayarjargal L, Morgenroth W, Winkler B, Ciezak-Jenkins J, Batyrev I G and Milman V 2014 *Chem. Eur. J.* **20** 11531
[31] Huang J, Blakemore J D, Fazi D, Kokhan O, Schley N D, Crabtree R H, Brudvig G W and Tiede D M 2014 *Phys. Chem. Chem. Phys.* **16** 1814
[32] Ekin J 2006 *Experimental Techniques for Low-Temperature Measurements: Cryostat Design, Material Properties and Superconductor Critical-Current Testing* (Oxford University Press)
[33] Rehr J J 2006 *Nature* **440** 618
[34] Juhas P, Cherba D M, Duxbury P M, Punch W F and Billinge S J L 2006 *Nature* **440** 655
[35] Shastri S D 2004 *J. Synchrotron Rad.* **11** 150
[36] Snigirev A and Snigireva I 2008 *C. R. Phys.* **9** 507
[37] Hong X G, Ehm L, Zhong Z, Ghose S, Duffy T S and Weidner D J 2016 *Sci. Rep.* **6** 21434
[38] Farrow C L, Shaw M, Kim H, Juhás P and Billinge S J L 2011 *Phys. Rev. B* **84** 134105
[39] Krishnan S and Price D L 2000 *J. Phys. -Condens. Matter* **12** R145
[40] Benmore C J 2012 *ISRN Mater. Sci.* **2012** 852905